Reconstitution of the complete rupture in musculotendinous junction using skeletal muscle-derived multipotent stem cell sheet-pellets as a “bio-bond”

Hiroyuki Hashimoto, Tetsuro Tamaki, Maki Hirata, Yoshiyasu Uchiyama, Masato Sato, Joji Mochida

Background. Significant and/or complete rupture in the musculotendinous junction (MTJ) is a challenging lesion to treat because of the lack of reliable suture methods. Skeletal muscle-derived multipotent stem cell (Sk-MSC) sheet-pellets, which are able to reconstitute peripheral nerve and muscular/vascular tissues with robust connective tissue networks, have been applied as a “bio-bond”. **Methods.** Sk-MSC sheet-pellets, derived from GFP transgenic-mice after 7 days of expansion culture, were detached with EDTA to maintain cell-cell connections. A completely ruptured MTJ model was prepared in the right tibialis anterior (TA) of the recipient mice, and was covered with sheet-pellets. The left side was preserved as a contralateral control. The control group received the same amount of the cell-free medium. The sheet-pellet transplantation (SP) group was further divided into two groups; as the short term (4-8 weeks) and long term (14-18 weeks) recovery group. At each time point after transplantation, tetanic tension output was measured through the electrical stimulation of the sciatic nerve. The behavior of engrafted GFP^+ tissues and cells was analyzed by fluorescence immunohistochemistry. **Results.** The SP short term recovery group showed average 64% recovery of muscle mass, and 36% recovery of tetanic tension output relative to the contralateral side. Then, the SP long term recovery group showed increased recovery of average muscle mass (77%) and tetanic tension output (49%). However, the control group showed no recovery of continuity between muscle and tendon, and demonstrated increased muscle atrophy, with coalescence to the tibia during 4-8 weeks after operation. Histological evidence also supported the above functional recovery of SP group. Engrafted Sk-MSCs primarily formed the connective tissues and muscle fibers, including nerve-vascular networks, and bridged the ruptured tendon-muscle fiber units, with differentiation into skeletal muscle cells, Schwann cells, vascular smooth muscle, and endothelial cells. **Discussion.** This bridging capacity between tendon and muscle fibers of the Sk-MSC sheet-pellet, as a “bio-bond”, represents a possible treatment for various MTJ ruptures following surgery.

Reconstitution of the complete rupture in musculotendinous junction using skeletal muscle-derived multipotent stem cell sheet-pellets as a "bio-bond"

Hiroyuki Hashimoto[1,2], Tetsuro Tamaki[2,3], Maki Hirata[1,2], Yoshiyasu Uchiyama[1,2], Masato Sato[1], Joji Mochida[1].

[1]Department of Orthopedics,

[2]Muscle Physiology and Cell Biology Unit,

[3]Department of Human Structure and Function,

Tokai University School of Medicine, 143 Shimokasuya, Isehara, Kanagawa 259-1193 Japan.

Correspondence to: Tetsuro Tamaki, PhD

Muscle Physiology and Cell Biology Unit, Department of Human structure and Function, Tokai University School of Medicine

143-Shimokasuya, Isehara, Kanagawa 259-1143 Japan.

Tel: +81-463-93-1121 (ext.2524); Fax: +81+463-95-0961

E-mail: tamaki@is.icc.u-tokai.ac.jp

ABSTRACT

Background. Significant and/or complete rupture in the musculotendinous junction (MTJ) is a challenging lesion to treat because of the lack of reliable suture methods. Skeletal muscle-derived multipotent stem cell (Sk-MSC) sheet-pellets, which are able to reconstitute peripheral nerve and muscular/vascular tissues with robust connective tissue networks, have been applied as a "bio-bond".

Methods. Sk-MSC sheet-pellets, derived from GFP transgenic-mice after 7 days of expansion culture, were detached with EDTA to maintain cell-cell connections. A completely ruptured MTJ model was prepared in the right tibialis anterior (TA) of the recipient mice, and was covered with sheet-pellets. The left side was preserved as a contralateral control. The control group received the same amount of the cell-free medium. The sheet-pellet transplantation (SP) group was further divided into two groups; as the short term (4-8 weeks) and long term (14-18 weeks) recovery group. At each time point after transplantation, tetanic tension output was measured through the electrical stimulation of the sciatic nerve. The behavior of engrafted GFP^+ tissues and cells was analyzed by fluorescence immunohistochemistry.

Results. The SP short term recovery group showed average 64% recovery of muscle mass, and 36% recovery of tetanic tension output relative to the contralateral side. Then, the SP long term recovery group showed increased recovery of average muscle mass (77%) and tetanic tension output (49%). However, the control group showed no recovery of continuity between muscle and tendon, and demonstrated increased muscle atrophy, with coalescence to the tibia during 4-8 weeks after operation. Histological evidence also supported the above functional recovery of SP group. Engrafted Sk-MSCs primarily formed the connective tissues and muscle fibers, including nerve-vascular networks, and bridged the ruptured tendon-muscle fiber units, with differentiation

into skeletal muscle cells, Schwann cells, vascular smooth muscle, and endothelial cells.

Discussion. This bridging capacity between tendon and muscle fibers of the Sk-MSC sheet-pellet, as a “bio-bond”, represents a possible treatment for various MTJ ruptures following surgery.

Key words: nerve reconstitution, vascular reconstitution, muscle regeneration, tendon regeneration, stem cell therapy.

INTRODUCTION

Skeletal muscles represent muscle-tendon complexes attached to the bone. However, due to their roles in the protection of the body and the force generation at the body-movements, injuries invariably occur during various activities or as a result of accidents. Muscle injuries can be classified as ruptures, tears, and lacerations, typically caused by external hard compression (contusion) or excessive stretching forces, and they are categorized into 3 grades of severity, as follows: Grade-I (mild) injury affects only a limited number of fibers in the muscle, and the strength does not decrease in the full active and passive range of motions, with pain and tenderness being delayed until the next day; Grade-II (moderate) injury, where nearly half of muscle fibers are torn, and acute and significant pain is accompanied by swelling and a minor decrease in muscle strength; Grade-III (severe) injury, with the complete rupture of the muscle, where the injured muscle is torn into 2 parts, together with severe swelling and pain, and a total loss of function. The injuries can be broadly divided according to their location in the muscle belly, musculotendinous junction (MTJ), and tendon tear (Chan et al. 2012; ElMaraghy & Devereaux 2012). Generally, for Grade-I and -II injuries, conservative treatments are usually applied, but in the case of Grade-III injuries, surgical intervention is often considered (Kragh et al. 2005c; Oliva et al. 2013; Rawson et al. 2013). Several suturing techniques have been reported for the treatment of complete tendon rupture (Hirpara et al. 2007; Maquirriain 2011; Merolla et al. 2009; Rawson et al. 2013; Yildirim et al. 2006), but there is a lack of reliable suture methods for the ruptures that involve the muscle belly or MTJ (Faibisoff & Daniel 1981; Kragh et al. 2005c; Oliva et al. 2013; Phillips & Heggers 1988). Complete rupture at the MTJ is particularly difficult, whereas suture of the muscle belly has been previously attempted (Kragh et al. 2005a; Kragh et al. 2005b; Kragh et al. 2005c). The maintenance of the continuity in muscle-tendon unit

is important, and strengthening of the adhesion properties is absolutely imperative, as there is a risk of repeated rupture after both surgical and/or non-surgical treatments (Kircher et al. 2010; Young et al. 2014).

Furthermore, tearing of the muscle-tendon unit can damage small blood vessels and nerves, generally causing local bleeding, pain, and/or paralysis. Therefore, the early re-establishment of peripheral nerve and blood vessels is important for the muscle repair process, in order to maintain the supply of O_2 and other nutrients, and the removal of CO_2 and other waste products (Ackermann et al. 2002; Ackermann et al. 2003; Nishimori et al. 2012). Additionally, it has been suggested that the repair of tendon ruptures can be stimulated by a single application of several growth factors, including platelet-derived growth factor (PDGF) (Hildebrand et al. 1998), transforming growth factor (TGF)-β (Kashiwagi et al. 2004), insulin-like growth factor (IGF)-1 (Kurtz et al. 1999), basic-fibroblast growth factor (bFGF) (Chan et al. 2000), and vascular endothelial growth factor (VEGF) (Zhang et al. 2003). Synchronized supply of these factors is considered beneficial for the reconstruction of the muscle-tendon unit.

Therefore, the application of an adhesive able to connect muscles to tendons may be a good treatment strategy for MTJ injury. Several scaffolds have been applied in the tendon healing treatments, and recent tissue-engineering investigations have shown that cell-scaffold constructs can improve the healing of tendon defects, compared with scaffolds alone (Ouyang et al. 2002; Ouyang et al. 2003; Young et al. 1998). Bone marrow-derived mesenchymal stem cells are most frequently applied as adjuvant cells, and their favorable healing effects have been reported (Chong et al. 2007; Ouyang et al. 2004; Ouyang et al. 2002; Ouyang et al. 2003), while the behavior of the transplanted cells, in terms of engraftment and differentiation, is poorly understood. We have determined that skeletal muscle-derived multipotent stem cells (Sk-MSCs)

are capable of synchronized reconstitution of muscle-nerve-blood vessel unit and cellular differentiation into skeletal muscle cells, Schwann cells, perineurial/endoneurial cells, pericytes, vascular smooth muscle cells, and endothelial cells (Tamaki et al. 2007a; Tamaki et al. 2005). Recently, we developed a 3D gel-patch tissue reconstitution system using Sk-MSC sheet-pellets, which are able to preferentially reconstitute peripheral nerve and vascular tissues with robust connective tissue networks (Tamaki et al. 2013). Sk-MSC sheet-pellets also expressed various neurotropic/neurotrophic and vasculogenic factor mRNAs before and after transplantation (Soeda et al. 2013; Tamaki et al. 2013). These properties of Sk-MSCs and their sheet-pellets are considered to be beneficial for the reconstitution of muscle-tendon units, including their nerve-blood vessel networks. In this study, we developed a complete rupture model for MTJ in tibialis anterior (TA) muscle of mice, and applied Sk-MSC sheet-pellets as a “bio-bond”-like substance. Functional recovery, which was evaluated by the electrical stimulation-induced muscle contractions via the sciatic nerve, was measured and the behavior of engrafted cells was analyzed immunohistochemically. The putative paracrine capacity of growth factors in the sheet-pellets, relating to skeletal muscle, nerve, and vascular regeneration, was confirmed by RT-PCR and protein array.

MATERIALS AND METHODS

Animals

Green fluorescent protein transgenic mice (GFP-Tg mice; C57BL/6 TgN[act EGFP]Osb Y01, provided by Dr. M. Okabe, Osaka University, Osaka, Japan) (Okabe et al. 1997) were used as donor mice for the cell transplantation experiments (male, 4-8 week old, n=5), and wild-type mice (C57BL/6N) were used as recipients (male, 8-12 week old, n=13). All experimental

113 procedures were approved by the Tokai University School of Medicine Committee on Animal
114 Care and Use (153015).

115 ***Cell Purification and Preparation of Stem Cell Sheet-Pellets***

116 Sk-MSC sheet-pellets (Tamaki et al. 2013) were investigated for their effects on the
117 regeneration of completely ruptured MTJ. Sheet-pellets generally showed gel-like characteristics,
118 and they were able to be lifted using forceps. The thigh and lower leg muscles (tibialis anterior,
119 extensor digitorum longus, soleus, plantaris, gastrocnemius, and quadriceps femoris) of GFP-Tg
120 mice were removed and used in subsequent experiments. Muscle sampling was performed under
121 an overdose of pentobarbital (60 mg/kg, Schering-Plough, combined with butorphanol tartrate 2
122 mg/kg, Meiji Seika, Tokyo, Japan, i.p.). Average total muscle mass removed during the procedure
123 was 512±67 mg/GFP-Tg mouse (mean±SE). Muscles were not minced, and were subsequently
124 treated with 0.1% collagenase type IA (Sigma-Aldrich, Tokyo, Japan) in Dulbecco's modified
125 Eagle's medium (DMEM, Wako, Osaka, Japan) containing 7.5% fetal calf serum (FCS, Equitech
126 Bio, TX, USA) with gentle agitation for 30 min at 37°C. Following a short digestion, whole
127 muscles were divided into fiber-bundles, which were washed with culture medium (Iscove's
128 modified Dulbecco's medium; IMDM, Wako, Osaka, Japan) containing 10% FCS, and cultured
129 in IMDM/20% FCS with 100 units/ml penicillin G, 100 μg/ml streptomycin sulfate (Wako,
130 Osaka, Japan), 10 μg/ml gentamycin sulfate (Schering-Plough, Osaka, Japan), and 0.1 mM β-
131 mercaptoethanol (Wako, Osaka, Japan) for 3 days. Cultured fiber-bundles associated with
132 expanded cells were treated with trypsin-EDTA (0.05% trypsin, 0.53 mM EDTA; Life
133 Technologies, Tokyo, Japan), in order to dissociate individual cells. Single-cell suspension was
134 filtered through 70-, 40- and 20-μm nylon filters in order to remove muscle fibers and other

debris, and, after washing, isolated cells were re-cultured in IMDM/20% FCS for 2-3 days, until they reached confluence. In total, cells were expanded in culture for 5-6 days, which represents a reduced culture time compared with previous studies (Soeda et al. 2013; Tamaki et al. 2013), thus preserving the myogenic potential of sheet-pellets. After they reached confluence, the cells were gently detached from culture dishes using 2 mM EDTA solution. This step mainly affected Ca^{2+}-dependent cell adhesion (e.g., cadherins), while cell-to-cell contact was maintained, sheet-like cell aggregations were collected and centrifuged, and stem cell sheet-pellets were obtained. Total sheet-pellet mass was 120±17 mg/mouse (mean±SE), which means that over 100 mg of sheet-pellets were obtained from about 500 mg of skeletal muscle tissue. Throughout cell isolation, 7.5-10% FCS was added to the collagenase and washing solutions in order to minimize contaminating protease activity and to protect isolated cells as much as possible.

RT-PCR and protein Analysis of the Sheet-pellets

Quality, differentiation potential and relative expressions of cytokines of the cells forming sheet-pellets was confirmed by RT-PCR and antibody array analysis immediately before the transplantation. Cells composed sheet-pellet was prepared for the RT-PCR, and their supernatant was prepared for antibody array analysis. For the RT-PCR analysis, specific primers and the analyzed materials are summarized in **Table 1**. Cells were lysed and total RNA was purified using a QIAGEN RNeasy Micro Kit (Hilden, Germany). First-strand cDNA synthesis was performed with Invitrogen SuperScript III system using dT30-containing primer (see Table 1), and specific PCR (35 cycles of 30 s at 94°C, 30 s at 60-65°C and 2 minutes at 72°C) was performed in a 15-μl volume containing Ex-Taq buffer, 0.8 U of ExTaq-HS-polymerase, 0.7 μM specific sense and antisense primers, 0.2 mM dNTPs, and 0.5 μl of cDNA. Relative expression

was normalized to the expression of a housekeeping control (HPRT). Details of this analysis were described previously (Tamaki et al. 2013).

Concurrently, several cytokines, which are related to the muscular and vascular regeneration were also analyzed by antibody array kit (Proteome Profiler, ARY013, R & D Systems, Minneapolis, MN), as a protein level. Cell culture supernatant of sheet-pellet just before the transplantation was obtained after removal of particulates by centrifugation, and 500-µl of supernates was prepared for the analysis. Culture medium containing 20% FCS was also prepared for the same analysis in order to check the background effects. The relative expression levels of several cytokines; such as interleukin-6 (IL-6), insulin-like growth factor-1 and 2 (IGF-1 and 2) and their related proteins IGF binding protein-1, 2, 5, and 6 (IGFBP-1, 2, 5 and 6), which are the critical regulator of myogenesis; a regulator/enhancer of macrophage such as chemokine (C-C motif) ligand 2 (MCP-1) and colony stimulating factor 1 (M-CSF); a regulator/activator of wide range of cell types such as fibroblast growth factor-21 (FGF-21) and tissue inhibitor of metalloproteinase 1 (TIMP-1); and vascular endothelial growth factor (VEGF) were determined.

Complete Rupture of MTJ Model and Application of Sheet-Pellets

In order to prepare the experimental complete rupture model, we manually detached muscle fibers from the distal tendons of the right tibialis anterior (TA) muscles of recipient mice (n=13). All surgical preparations were performed under the inhalation anesthesia (Isoflurane; Abbot, Osaka, Japan). A summary of the procedure is shown in **Figure 1**. First, TA muscle was exposed (A, step 1), and muscle fibers were subsequently detached from the distal tendon and peeled off using cotton swabs for one half of the entire TA length (B, step 2), and everted necrotic fiber portions were removed (step 3). The average removed muscle mass was 21.5±1.8 g, and this

represented about 40% of total muscle mass. Sheet-pellets were then adhered to the open region of completely ruptured MTJ (**Fig. 1C**, step 4; Sheet-pellet, SP group, n=8), and skin was sutured (C, white arrows). The left side was preserved as a contralateral control. The non-transplanted control group (C group, n=5) underwent the same surgery, and the same amount of cell-free culture medium was administered. The mice were allowed full freedom of movement after surgery.

Functional Assessment of the Regenerated TA Muscles

After the transplantation, the animals were divided into two groups as short (4-8 weeks) and long (14-18 weeks) term recoveries, and prepared for the functional assessment. The first assessment was begun at 4 weeks using each one mouse in SP and C group, and Tetanic tension outputs of regenerated TA muscles were measured in both left (non-operated control side) and right (operated side) legs. Following assessments were performed every week (1-1.5 week interval) during each group terms using one by one mouse, then, SP and C groups were compared. Measurements were performed *in situ* under inhalation anesthesia (Isoflurane; Abbot, Osaka, Japan), and body (rectal) temperature was maintained at 36±1°C with a radiant heat light throughout the measurement. Details of this measurement were as described previously (Tamaki et al. 2005). Briefly, the distal tendon of TA muscle and sciatic nerve (about 10 mm) on both sides were carefully exposed, and tissues were coated with mineral oil to prevent tissue drying and to minimize electrical noise interference. A bipolar silver (Ag/Ag) electrode (inter-electrode distance: 2 mm) was placed under the sciatic nerve. A stainless steel hook was attached to the distal tendon of each TA muscle using a silk ligature. The animal was transferred to a custom-made operating table that allowed stabilization of the head and limbs in a supine position using

surgical tape. A stainless steel hook was attached to a force-distance transducer (FD-Pickup, TB-611T; Nihon Kohden, Tokyo, Japan) connected to the carrier amplifier (AP-621G; Nihon Kohden). This enabled the measurements of the muscle contraction force and its distance to be conducted. A bipolar silver electrode (inter-electrode distance: 5 mm/1 mm diameter) was attached to the surface of the reference muscle as well, in order to obtain an evoked electrical myogram, as a confirmation of stable muscle contractions. We have taken care to avoid interference of the reference muscle and nerves with the normal blood supply. Afterward, twitches were elicited by single pulse (1 ms duration, 0.5 Hz) electrical stimulation via the sciatic nerve, at a voltage above the threshold for a maximum response (1.5-4.0 V). Subsequently, peak tetanic tension was determined using stimulation frequencies of 10, 20, 40, 60, 80, 100, 120, and 140 Hz of 0.5 s duration at 15 s intervals. The frequency that produced the highest tetanic tension was considered the optimal stimulation for tetanus. All mechanical and electrical measurements were recorded on a Linearcorder (Mark VII, WR3101; Graphtec, Tokyo, Japan) as analog data. The tetanic tension output was considered as the total functional recovery of the operated TA muscle, and recovery ratio was determined based on the contralateral non-operated control side. The same functional measurements were also performed at 10 weeks post-transplantation, in order to assess the progress of recovery.

Macroscopic Observation and Immunostaining

Following the functional measurements above, recipient mice (including the animals used for morphological analysis only, 5-10 weeks after transplantation, n=5) were given an overdose of pentobarbital (60 mg/kg, combined with butorphanol tartrate 2 mg/kg, i.p.), and the engraftment of donor-derived GFP^+ cells into the damaged portion of TA muscle was confirmed by fluorescence stereomicroscopy (SZX12; Olympus, Tokyo, Japan, **Figure 4**). Recipient mice were perfused with warm 0.01 M phosphate-buffered saline (PBS, Wako, Osaka, Japan) through the left ventricle, followed by fixation with 4% paraformaldehyde /0.1 M phosphate buffer (4% PFA/PB, Wako, Osaka, Japan). Muscles were removed and fixed overnight in 4% PFA/PB, washed with graded sucrose (0-25%, Wako, Osaka, Japan)/0.01 M PBS series, and quick frozen with isopentane (Wako, Osaka, Japan) pre-cooled by liquid nitrogen, followed by storage at -80°C. Subsequently, 7 μm cross-sections were obtained. Skeletal muscle fibers were stained with anti-skeletal muscle actin (αSkMA; dilution, 1:200; incubation, room temperature for 2 h; Abcam, Cambridge, UK). Nerve fiber localization (axons) was detected by rabbit polyclonal anti-Neurofilament 200 (N-200, dilution, 1:1000; incubation, room temperature for 1 h; Sigma, St. Louis, MO, USA). Schwann cells were detected using anti-p75 (rabbit polyclonal, 1:400, 4°C overnight; CST, Boston, MA, USA). Blood vessels were detected with rat anti-mouse CD31 (1:500, 4°C overnight; BD Pharmingen, San Diego, CA, USA) monoclonal antibody, which is a known vascular endothelial cell marker, and mouse monoclonal α-smooth muscle actin (αSMA, Cy3-conjugated; 1:1500; room temperature for 1 h; Sigma, St. Louis, MO, USA). Dystrophin formation in the skeletal muscle fibers was detected using goat anti-dystrophin polyclonal antibody (1:50, 4°C, overnight; Santa Cruz Biotechnology, Dallas, TX, USA). Neuromuscular junctions were detected by α-bungarotoxin (Alexa Fluor 594 conjugated, 1:100, room temperature,1 h; Molecular Probes, Eugene, OR, USA). Reactions were visualized using Alexa

Fluor-594-conjugated goat anti-rabbit and anti-rat antibodies (1:500, room temperature, 2 h; Molecular Probes, Eugene, OR, USA). Nuclei were counter-stained with DAPI (4,6-diamino-2-phenylindole).

Statistical Analysis

Differences between two groups (short and long term recovery group) were tested using Student's t test, and the significance level was set at $p<0.05$. Values are expressed as mean ± SE.

RESULTS

Quality and Therapeutic Potential of Sk-MSC Sheet-pellets

Quality, differentiation, and putative therapeutic potential of the sheet-pellet were first confirmed by RT-PCR and protein array analysis (**Figure 2**). The expression of specific myogenic, neurotrophic, and vasculogenic factor mRNAs in the sheet-pellets immediately before the transplantation is shown in **Figure 2A**. The Sk-MSC sheet-pellets showed expressions of various myogenic factors (MyoD, Myf5, Pax7, Myogenin, c-met, Mcad, MyH, Desmin, and IGF-1), neurotrophic factors (NGF, BDNF, GDNF, CNTF, LIF, Ninjurin, Galectin, Nestin, and Sox10) and vascular growth factors (VEGF, HGF, PDGF, TGF-β, EGF, and FGFb), except Pax3. These results agree with a previous report (Tamaki et al. 2013), which showed good quality of this method of sheet-pellet preparation.

In addition, relative increase in the expressions of proteins (cytokines) was also detected in the same sheet-pellet culture supernatant (**Figure 2B**). An increase of myokine (Munoz-Canoves et al. 2013; Pedersen 2012), which is a critical regulator of muscle regeneration, such as

IL-6 and IGF-1 and 2 associate with their relating IGFBP-2, 3, 5 and 6, the chemokine, which is an up-regulator of monocyte/macrophage (MCP-1 and M-CSF) in the tissue regeneration (Pantsulaia et al. 2005; Shiba et al. 2007), and a regulator/activator of a wide range of cell types (FGF-21 and TIMP-1) (Mas et al. 2007; Wan 2013) was detected, showing a paracrine capacity of the sheet-pellet.

Functional Recovery

The results of functional assessment are summarized in **Table 2**. The SP short term recovery group showed average 64% recovery of muscle mass, and 36% recovery of tetanic tension output relative to the contralateral side. Then, the SP long term recovery group showed increased recovery of average muscle mass (77%) and tetanic tension output (49%). The age-dependent increase in muscle mass was also observed between short (4-8 weeks) and long (14-18 weeks) term recovery group (45.2±5.8 to 50.4±0.5mg). Importantly, the control group did not recover the continuity of the muscle-tendon unit, and the remaining muscles showed atrophy with coalescence into the tibial bone in the short term group (see next **Fig. 4I and J**), thus showing that this model is irreversible spontaneously. Therefore, we were unable to continue measuring muscle mass and tension output in the Control group subsequently.

Differences of operated-muscle mass and tetanic tension recoveries between the short and long term groups, and these composed individual plots at each measurement point are also shown in **Figure 3**. Average of muscle mass and tension output were both higher in the long term group (**Fig. 3A, B**), showing that a development of recoveries continued over 14 weeks after operation. On the individual plot, a term depends manner of recoveries were clearly observed in the long term group as a linear relationship, but not in the short term group (**Fig. 3C and D**). This

may be representing the effect of standard body activities of mice in the cages, because general activities (go around, hanging and downside walking of cage lid) were clearly higher in the long term recovery group than that in the short term group by our animal care observations (data not shown).

Macroscopic Examination

Typical fluorescence macroscopic features at 4-10 weeks after the engraftment of transplanted GFP^+ sheet-pellets are shown in **Figure 4**. *In situ* observation revealed that a large volume of GFP^+ tissues was engrafted in the damaged TA muscle portion after transplantation, and these tissues showed 5 different patterns. Pattern 1 was the most common one (5/13 samples), showing broad and thick engraftment through the tendon to the mid portion of the muscle (**Figs. 4A-C**). GFP^+ engrafted tissue was observed in blood vessel networks (arrows in **Fig. 4B**), and the continuity was clearly maintained (**Fig. 4C**). This pattern was mainly composed of connective tissue with few muscle fibers. Pattern 2 was rarely observed (1/13 samples), and it mostly comprised of the muscle fibers (**Fig. 4D**) that extended from the mid portion of MTJ to the upper portion, and with few connective tissues. Pattern 3 (1/13 samples) in contrast, mainly comprised of the connective tissue at the distal portion of MTJ, with few muscle fibers (**Fig. 4E**). Patterns 4 (3/13 samples) and 5 (3/13 samples) were mixed types, showing both muscle fibers and connective tissues (**Figs. 4F-H**), but GFP was relatively sparse, and the amount of connective tissues was small in Pattern 4 (**Fig. 4F**), while Pattern 5 showed even distribution of both tissues (**Fig. 4G**). Active blood vessels in and around GFP^+ tissues were equally observed in all Patterns (arrows in **Figs. 4B, and 4D-4H**).

Severe atrophy of TA muscle was generally observed in the C group (**Figs. 4I** and **4J**), and this

306 pattern was observed in 5/5 control mice. On the lateral side of the tibia (black arrows in **Figs. 4I**
307 and **4J**), a portion of the TA muscle was clearly hollowed (white arrows in **Fig. 4I**), and there
308 were no muscle fibers present. Apparent adipose tissue formation (red arrows in **Fig. 4J**) was also
309 observed, suggesting discontinuity of the TA muscle-tendon unit (**Fig. 4J**).

310 ***Immunohistochemical Analysis of the Engrafted Cells***

311 At 4-10 weeks following the surgery, the behavior of engrafted GFP^+ cells was analyzed
312 in cross-sections. **Figure 5** shows the result of Pattern 1. Thick tissues composed of GFP^+ cells
313 closely adhered to skeletal muscle fibers (**Fig. 5A**). GFP^+ cells surrounded the tendon, and van
314 Gieson elastic fiber staining showed connective tissue networks (**Fig. 5B**). This suggests that the
315 engrafted GFP^+ tissue formed connective tissue networks, which connected both the tendon and
316 the muscle fibers, displaying a "bio-bond" role. Additionally, GFP^+ cells were observed in the
317 tendon (yellow arrows in **Fig. 5C**), and showed differentiation into vascular endothelial cells
318 (CD31 + GFP, white arrows in **5C**). A similar trend was also observed on the muscle fiber side,
319 and the migration of GFP^+ cells could be seen between muscle fibers (**Fig. 5D**, below the dotted
320 line). A close relationship (not double staining) of $N200^+$ nerve axons and GFP^+ cells, was
321 observed on both the muscle side (below the dotted line) and the connective tissue side (**Fig. 5D**,
322 upper-side of dotted line). GFP^+ cells in the connective tissue were positive for p75 (**Fig. 5E**,
323 right side of dotted line) and therefore, they were considered Schwann cells. These results
324 support a close relationship between GFP^+ cells and nerve axons, which is detectable in **Figure**
325 **5D**. The relationship among engrafted GFP^+ connective tissue, tendon, and muscle fibers is more
326 apparent in **Figure 4F**. GFP^+ connective tissue bridging tendon (T) and muscle fibers (right side
327 of the panel) expressed dystrophin (red), which suggests a strong relationship between connective

tissue and muscle fibers through dystrophin complexes.

Similarly, longitudinal profiles obtained from pattern 5 are shown in **Figure 6**. Engrafted GFP^+ cell-derived connective tissues closely adhered to the muscle fibers (**Fig. 6A**), and GFP^+ muscle fibers were also observed (**Fig. 6B**). Differentiation of GFP^+ cells into vascular smooth muscle cells was seen in the connective tissue network (**Fig. 6C**, arrows, double staining with GFP+SMA), contributing to a relatively large blood vessel formation. The involvement in the peripheral nerve reconstitution was indicated by a close relationship between GFP^+ cells and axons (**Fig. 6D**, arrows, close distributions of GFP^+ cells and $N200^+$ axons). This relationship was supported by the differentiation of GFP^+ cells into Schwann cells positive for p75 (**Fig. 6E**, arrows, double staining of GFP+p75). Similarly, a close relationship of GFP^+ cells and muscle fibers, nerve axons, and the neuromuscular junctions was evident (**Fig. 6F**, in the dotted line circle as α-bungarotoxin$^+$), confirming that GFP^+ cells contributed to peripheral nerve extensions, reaching to the end of a motor nerve. These results indicate that the transplanted GFP^+ Sk-MSC sheet-pellets mainly form connective tissue networks together with a certain amount of muscle fibers, and that they physically bind the tendon and muscle fibers, contributing to the peripheral nerve-blood vessel formation.

DISCUSSION

Injuries involving the muscle belly or MTJ are challenging for surgeons because the muscle tissue shows poor suture-holding capacity, and the reliable suture methods have not been established yet (Faibisoff & Daniel 1981; Kragh et al. 2005c; Oliva et al. 2013; Phillips & Heggers 1988). However, reconstruction and/or re-establishment of continuity in the muscle-

tendon unit is vital for the functional repair, because of the primary role of muscle force generation and transmission. We have investigated the reconstruction of completely ruptured TA muscle at the MTJ, using Sk-MSC sheet-pellets as "bio-bonds." The results indicate that Sk-MSC sheet-pellet transplantation achieved favorable results in the reconstruction and/or reconnection of the ruptured muscles and tendons. Engrafted Sk-MSCs primarily formed connective tissues, including neurovascular networks, and bridged both the tendon and muscle fibers, with differentiation into skeletal muscle fibers, Schwann cells, vascular smooth muscles, and endothelial cells. The differentiation capacity of these cells was previously predicted, since the present sheet-pellet was mainly composed of the mixed population of multipotent Sk-34 ($CD34^+/45^-$) (Tamaki et al. 2002; Tamaki et al. 2005) and Sk-DN ($CD34^-/45^-$) (Tamaki et al. 2003; Tamaki et al. 2007a; Tamaki et al. 2007b) cells, and their putative potential for the therapy was confirmed by RT-PCR and protein array analysis immediately before the transplantation (**Fig. 2A and B**). Furthermore, the migration of engrafted GFP^+ fibroblast-like cells was observed around the tendon and the interstitium of muscle fibers, mechanically bridging the tendon-muscle gap. This reconnecting behavior is considered the “bio-bond” activity. Establishment of a muscle fiber holding capacity in donor-derived connective tissue was further suggested by the expression of dystrophin in MTJ fibers (**Fig. 5F**), because of the role of dystrophin-dystroglycan (α, β) complex in the collagen network (Monti et al. 1999; Welser et al. 2009). In our previous studies, we prepared the sheet-pellets as the accelerators of the neurovascular reconstitution with diminished myogenic potential (Soeda et al. 2013; Tamaki et al. 2013). Here, we used a shorter term expansion culture (in particular, the term of first fiber culture), and this shorter culture period helped preserve the myogenic potential of the sheet-pellets, resulting in new myofiber formation. This was confirmed by the comparison of the RT-PCR data obtained in the previous studies

(Soeda et al. 2013; Tamaki et al. 2013) and the results obtained in this one (**Fig. 2**). The relatively preserved myofiber formation capacity may have also contributed to the enhanced connection of the muscle-tendon unit.

The investigated sheet-pellets contributed to functional regeneration of disrupted TA muscles by 36% in the short term recovery group, and this increased 49% in the long term recovery group. Concerning to the relationship between the engrafted patterns (**Fig. 4**) and functions, relatively higher contractions were dominantly observed in the Pattern 4 and 5 (**Fig. 4F** and **G**), which showed mixed types of GFP engraftment of both muscle fibers and connective tissues. The tension recoveries were further supported by the immunohistochemical staining results, showing that GFP^+ cells contributed to motor nerve extensions, close to the neuromuscular junctions (**Fig. 6F,** from Pattern 5). We did not perform the tensile strength test of the regenerated muscles, but no muscle ruptures were observed during repetitive maximum tetanic tension measurements. In addition, the absolute value of the tension output of operated-muscles (around 38 g) was superior to the mean body weight (around 34 g) in the long term group. Therefore, we believe that the tensile strength of operated-muscle may have been sufficient to support standard body activities, and it could be enhanced, as one type of rehabilitation, which resulted in an increased tension recovery in the long term group (**Table 2 and Fig. 3A, B**). The notion of this rehabilitation (increased body activity) depends increase in the tension recovery was further suggested by the term dependent linear relationship, as was observed particularly in the individual plots of the long term group (**Fig. 3D**). Because we observed enhanced general cage activities of the mice in the long term group compared to the short term group, and the same trend was also detected clearly in the muscle mass recovery (**Fig. 3C**). Thus, we believe that this linear relationship may be due to an increased general activity of

mice day by day following the improvement in the general symptoms, such as reduced pain and uncomfortable feeling. In this regard, it was suggested that these symptoms were more prominent in the short term group, and may induce lower activities. However, this lower activity might be a benefit for tissue recovery by contraries. By these reasons, it was also suggested that an earlier start of positive rehabilitation, probably around 8 weeks after operation, may have more rapid and enhanced recovery of this therapy was expected.

As a consequence, the non-transplanted control group did not achieve reconnection of muscle-tendon units (**Fig. 4** and **Table 2**), showing that the MTJ rupture model we used is an irreversible model. It has been reported that the early reconnection induced mechanical stimulation is effective for the repair and quality maintenance of the tendon, because the lack of this stimulation produced detrimental effects (Lin et al. 2004; Matsumoto et al. 2003). Therefore, we concluded that the absence of mechanical-tension in the control group, after the complete removal of the MTJ, may have caused a massive muscle atrophy associated with the fatty tissue replacement (**Fig. 4**). It is also a fact that the present sheet-pellets transplantation prevented this detrimental effects.

Additionally, it has been suggested that early peripheral nerve regeneration and the provision of neuropeptides are important for the healing of normal connective tissue and tendon (Ackermann et al. 2002; Ackermann et al. 2003). Neovascularization plays a critical role in the healing process of the ligament (Nishimori et al. 2012). The repair of angiokinesis (vasodilation-constriction) through the neurovascular regeneration is also important for tissue regeneration (Ackermann et al. 2002). Our treatment meets all these conditions. Previous studies demonstrated that Sk-MSCs transplantation facilitates/accelerates nerve-vascular formation (Tamaki et al. 2014; Tamaki et al. 2007a; Tamaki et al. 2013; Tamaki et al. 2005). The expressions of various

418 nerve-blood vessel-related growth and trophic factors before and after transplantation was also
419 observed in the case of nerve-gap regeneration (Tamaki et al. 2014). In our study, prolonged
420 expression of these genes, shown in **Figure 2**, was expected and observed following the
421 transplantation, and it may be beneficial for the healing of muscle-tendon units.
422 We recently established a practical/therapeutic method of isolation of human skeletal muscle-
423 derived stem cells (Tamaki et al. 2015). Using this method, we found that human cells can be
424 divided into 2 stem/progenitor cell fractions; 1) the cells showing preferential differentiation into
425 the skeletal myogenic lineage ($CD45^-/CD34^-/29^+$ = Sk-DN/29^+), and 2) cells showing multiple
426 differentiation into nerve-blood vessel cell lineages ($CD45^-/34^+$ = Sk-34). The combined
427 differentiation/reconstitution capacities of these cells after *in vivo* transplantation were
428 comparable to the mouse Sk-MSCs (Tamaki et al. 2015). Therefore, the cell fractions could be
429 selected and adjusted for the treatment of muscle fibers, nerve-blood vessels associated with
430 connective tissues, or both. Additionally, these stem/progenitor cells can be obtained from various
431 muscle regions, including the legs and abdominals (Tamaki et al. 2015). The removal of a small
432 sample (around 3 g) from the lower abdominal wall muscle carries low risk to the loss of motor
433 function.

434 **CONCLUSIONS**

435 In the present study, we successfully demonstrated that Sk-MSC sheet-pellet
436 transplantation can bridge complete rupture of MTJ, and form connective tissue networks
437 associated with cellular differentiation into skeletal muscle fibers, Schwann cells, vascular
438 smooth muscle, and endothelial cells. These connective tissues migrated around the tendon and
439 muscle fiber interstitium and connected both tissues, playing a role of a "bio-bond." Paracrine

effects of nerve and vascular growth factors, as well as trophic factors, produced by Sk-MSCs may also be beneficial for the reparation of the tissue. Together with the recent establishment of human skeletal muscle-derived cells, Sk-MSCs may be an optimal autologous cell source, used as an adjuvant, which would lead to a promising therapy for muscle-tendon injuries. Furthermore, the combined therapies, such as an appropriate suture with sheet-pellet, or suture together with sheet-pellet and scaffold use, may also represent favorable therapies for the MTJ rupture repair, particularly because of the higher tensile strength required in humans.

REFERENCES

Ackermann PW, Ahmed M, and Kreicbergs A. 2002. Early nerve regeneration after achilles tendon rupture--a prerequisite for healing? A study in the rat. *J Orthop Res* 20:849-856. 10.1016/S0736-0266(01)00159-0

Ackermann PW, Li J, Lundeberg T, and Kreicbergs A. 2003. Neuronal plasticity in relation to nociception and healing of rat achilles tendon. *J Orthop Res* 21:432-441. 10.1016/S0736-0266(02)00207-3

Chan BP, Fu S, Qin L, Lee K, Rolf CG, and Chan K. 2000. Effects of basic fibroblast growth factor (bFGF) on early stages of tendon healing: a rat patellar tendon model. *Acta Orthop Scand* 71:513-518. 10.1080/000164700317381234

Chan O, Del Buono A, Best TM, and Maffulli N. 2012. Acute muscle strain injuries: a proposed new classification system. *Knee Surg Sports Traumatol Arthrosc* 20:2356-2362. 10.1007/s00167-012-2118-z

Chong AK, Ang AD, Goh JC, Hui JH, Lim AY, Lee EH, and Lim BH. 2007. Bone marrow-derived mesenchymal stem cells influence early tendon-healing in a rabbit achilles tendon model. *J Bone Joint Surg Am* 89:74-81. 10.2106/JBJS.E.01396

ElMaraghy AW, and Devereaux MW. 2012. A systematic review and comprehensive classification of pectoralis major tears. *J Shoulder Elbow Surg* 21:412-422. 10.1016/j.jse.2011.04.035

Faibisoff B, and Daniel RK. 1981. Management of severe forearm injuries. *Surg Clin North Am* 61:287-301.

Hildebrand KA, Woo SL, Smith DW, Allen CR, Deie M, Taylor BJ, and Schmidt CC. 1998. The

effects of platelet-derived growth factor-BB on healing of the rabbit medial collateral ligament. An in vivo study. *Am J Sports Med* 26:549-554.

Hirpara KM, Sullivan PJ, Raheem O, and O'Sullivan ME. 2007. A biomechanical analysis of multistrand repairs with the Silfverskiold peripheral cross-stitch. *J Bone Joint Surg Br* 89:1396-1401. 10.1302/0301-620X.89B10.19360

Kashiwagi K, Mochizuki Y, Yasunaga Y, Ishida O, Deie M, and Ochi M. 2004. Effects of transforming growth factor-beta 1 on the early stages of healing of the Achilles tendon in a rat model. *Scand J Plast Reconstr Surg Hand Surg* 38:193-197. 10.1080/02844310410029110

Kircher J, Ziskoven C, Patzer T, Zaps D, Bittersohl B, and Krauspe R. 2010. Surgical and nonsurgical treatment of total rupture of the pectoralis major muscle in athletes: update and critical appraisal. *Open Access J Sports Med* 1:201-205. 10.2147/OAJSM.S9066

Kragh JF, Jr., Svoboda SJ, Wenke JC, Brooks DE, Bice TG, and Walters TJ. 2005a. The role of epimysium in suturing skeletal muscle lacerations. *J Am Coll Surg* 200:38-44. 10.1016/j.jamcollsurg.2004.09.009

Kragh JF, Jr., Svoboda SJ, Wenke JC, Ward JA, and Walters TJ. 2005b. Epimysium and perimysium in suturing in skeletal muscle lacerations. *J Trauma* 59:209-212.

Kragh JF, Jr., Svoboda SJ, Wenke JC, Ward JA, and Walters TJ. 2005c. Suturing of lacerations of skeletal muscle. *J Bone Joint Surg Br* 87:1303-1305. 10.1302/0301-620X.87B9.15728

Kurtz CA, Loebig TG, Anderson DD, DeMeo PJ, and Campbell PG. 1999. Insulin-like growth factor I accelerates functional recovery from Achilles tendon injury in a rat model. *Am J Sports Med* 27:363-369.

Lin TW, Cardenas L, and Soslowsky LJ. 2004. Biomechanics of tendon injury and repair. *J Biomech* 37:865-877. 10.1016/j.jbiomech.2003.11.005

Maquirriain J. 2011. Achilles tendon rupture: avoiding tendon lengthening during surgical repair and rehabilitation. *Yale J Biol Med* 84:289-300.

Mas VR, Maluf DG, Archer KJ, Yanek KC, and Fisher RA. 2007. Angiogenesis soluble factors as hepatocellular carcinoma noninvasive markers for monitoring hepatitis C virus cirrhotic patients awaiting liver transplantation. *Transplantation* 84:1262-1271. 10.1097/01.tp.0000287596.91520.1a

Matsumoto F, Trudel G, Uhthoff HK, and Backman DS. 2003. Mechanical effects of immobilization on the Achilles' tendon. *Arch Phys Med Rehabil* 84:662-667.

Merolla G, Campi F, Paladini P, and Porcellini G. 2009. Surgical approach to acute pectoralis major tendon rupture. *G Chir* 30:53-57.

Monti RJ, Roy RR, Hodgson JA, and Edgerton VR. 1999. Transmission of forces within mammalian skeletal muscles. *J Biomech* 32:371-380.

505 Munoz-Canoves P, Scheele C, Pedersen BK, and Serrano AL. 2013. Interleukin-6 myokine
506 signaling in skeletal muscle: a double-edged sword? *FEBS J* 280:4131-4148.
507 10.1111/febs.12338
508 Nishimori M, Matsumoto T, Ota S, Kopf S, Mifune Y, Harner C, Ochi M, Fu FH, and Huard J.
509 2012. Role of angiogenesis after muscle derived stem cell transplantation in injured
510 medial collateral ligament. *J Orthop Res* 30:627-633. 10.1002/jor.21551
511 Okabe M, Ikawa M, Kominami K, Nakanishi T, and Nishimune Y. 1997. 'Green mice' as a source
512 of ubiquitous green cells. *FEBS Lett* 407:313-319. S0014-5793(97)00313-X [pii]
513 Oliva F, Via AG, Kiritsi O, Foti C, and Maffulli N. 2013. Surgical repair of muscle laceration:
514 biomechanical properties at 6 years follow-up. *Muscles Ligaments Tendons J* 3:313-317.
515 Ouyang HW, Goh JC, and Lee EH. 2004. Use of bone marrow stromal cells for tendon graft-to-
516 bone healing: histological and immunohistochemical studies in a rabbit model. *Am J*
517 *Sports Med* 32:321-327.
518 Ouyang HW, Goh JC, Mo XM, Teoh SH, and Lee EH. 2002. The efficacy of bone marrow
519 stromal cell-seeded knitted PLGA fiber scaffold for Achilles tendon repair. *Ann N Y Acad*
520 *Sci* 961:126-129.
521 Ouyang HW, Goh JC, Thambyah A, Teoh SH, and Lee EH. 2003. Knitted poly-lactide-co-
522 glycolide scaffold loaded with bone marrow stromal cells in repair and regeneration of
523 rabbit Achilles tendon. *Tissue Eng* 9:431-439. 10.1089/107632703322066615
524 Pantsulaia I, Trofimov S, Kobyliansky E, and Livshits G. 2005. Contribution of the familial and
525 genetic factors on monocyte chemoattractant protein-1 variation in healthy human
526 pedigrees. *Cytokine* 32:117-123. 10.1016/j.cyto.2005.08.006
527 Pedersen BK. 2012. Muscular interleukin-6 and its role as an energy sensor. *Med Sci Sports*
528 *Exerc* 44:392-396. 10.1249/MSS.0b013e31822f94ac
529 Phillips LG, and Heggers JP. 1988. Layered closure of lacerations. *Postgrad Med* 83:142-148.
530 Rawson S, Cartmell S, and Wong J. 2013. Suture techniques for tendon repair; a comparative
531 review. *Muscles Ligaments Tendons J* 3:220-228.
532 Shiba Y, Takahashi M, Yoshioka T, Yajima N, Morimoto H, Izawa A, Ise H, Hatake K, Motoyoshi
533 K, and Ikeda U. 2007. M-CSF accelerates neointimal formation in the early phase after
534 vascular injury in mice: the critical role of the SDF-1-CXCR4 system. *Arterioscler*
535 *Thromb Vasc Biol* 27:283-289. 10.1161/01.ATV.0000250606.70669.14
536 Soeda S, Tamaki T, Hashimoto H, Saito K, Sakai A, Nakajima N, Nakazato K, Masuda M, and
537 Terachi T. 2013. Functional Nerve-Vascular Reconstitution of the Bladder-Wall;
538 Application of Patch Transplantation of Skeletal Muscle-Derived Multipotent Stem Cell
539 Sheet-Pellets. *J Stem Cell Res Ther* 3:142.
540 Tamaki T, Akatsuka A, Ando K, Nakamura Y, Matsuzawa H, Hotta T, Roy RR, and Edgerton VR.

2002. Identification of myogenic-endothelial progenitor cells in the interstitial spaces of skeletal muscle. *J Cell Biol* 157:571-577.

Tamaki T, Akatsuka A, Okada Y, Matsuzaki Y, Okano H, and Kimura M. 2003. Growth and differentiation potential of main- and side-population cells derived from murine skeletal muscle. *Exp Cell Res* 291:83-90.

Tamaki T, Hirata M, Soeda S, Nakajima N, Saito K, Nakazato K, Okada Y, Hashimoto H, Uchiyama Y, and Mochida J. 2014. Preferential and comprehensive reconstitution of severely damaged sciatic nerve using murine skeletal muscle-derived multipotent stem cells. *PLoS One* 9:e91257. 10.1371/journal.pone.0091257

PONE-D-13-38421 [pii]

Tamaki T, Okada Y, Uchiyama Y, Tono K, Masuda M, Wada M, Hoshi A, and Akatsuka A. 2007a. Synchronized reconstitution of muscle fibers, peripheral nerves and blood vessels by murine skeletal muscle-derived CD34(-)/45 (-) cells. *Histochem Cell Biol* 128:349-360. 10.1007/s00418-007-0331-5

Tamaki T, Okada Y, Uchiyama Y, Tono K, Masuda M, Wada M, Hoshi A, Ishikawa T, and Akatsuka A. 2007b. Clonal multipotency of skeletal muscle-derived stem cells between mesodermal and ectodermal lineage. *Stem Cells* 25:2283-2290. 2006-0746 [pii]

10.1634/stemcells.2006-0746

Tamaki T, Soeda S, Hashimoto H, Saito K, Sakai A, Nakajima N, Masuda M, Fukunishi N, Uchiyama Y, Terachi T, and Mochida J. 2013. 3D reconstitution of nerve-blood vessel networks using skeletal muscle-derived multipotent stem cell sheet pellets. *Regen Med* 8:437-451. 10.2217/rme.13.30

Tamaki T, Uchiyama Y, Hirata M, Hashimoto H, Nakajima N, Saito K, Terachi T, and Mochida J. 2015. Therapeutic isolation and expansion of human skeletal muscle-derived stem cells for the use of muscle-nerve-blood vessel reconstitution. *Front Physiol* 6:165. 10.3389/fphys.2015.00165

Tamaki T, Uchiyama Y, Okada Y, Ishikawa T, Sato M, Akatsuka A, and Asahara T. 2005. Functional recovery of damaged skeletal muscle through synchronized vasculogenesis, myogenesis, and neurogenesis by muscle-derived stem cells. *Circulation* 112:2857-2866.

Wan Y. 2013. Bone marrow mesenchymal stem cells: fat on and blast off by FGF21. *Int J Biochem Cell Biol* 45:546-549. 10.1016/j.biocel.2012.12.014

Welser JV, Rooney JE, Cohen NC, Gurpur PB, Singer CA, Evans RA, Haines BA, and Burkin DJ. 2009. Myotendinous junction defects and reduced force transmission in mice that lack alpha7 integrin and utrophin. *Am J Pathol* 175:1545-1554. 10.2353/ajpath.2009.090052

Yildirim Y, Saygi B, Kara H, Cabukoglu C, and Esemenli T. 2006. [Tendon holding capacities of the suture materials used in repairing Achilles tendon rupture]. *Acta Orthop Traumatol*

Turc 40:164-168.

Young RG, Butler DL, Weber W, Caplan AI, Gordon SL, and Fink DJ. 1998. Use of mesenchymal stem cells in a collagen matrix for Achilles tendon repair. *J Orthop Res* 16:406-413. 10.1002/jor.1100160403

Young SW, Patel A, Zhu M, van Dijck S, McNair P, Bevan WP, and Tomlinson M. 2014. Weight-Bearing in the Nonoperative Treatment of Acute Achilles Tendon Ruptures: A Randomized Controlled Trial. *J Bone Joint Surg Am* 96:1073-1079. 10.2106/JBJS.M.00248

Zhang F, Oswald T, Lin S, Cai Z, Lei M, Jones M, Angel MF, and Lineaweaver WC. 2003. Vascular endothelial growth factor (VEGF) expression and the effect of exogenous VEGF on survival of a random flap in the rat. *Br J Plast Surg* 56:653-659.

FIGURE LEGENDS

Figure 1. Macroscopic and schematic images of procedures used in MTJ complete rupture model preparation and sheet-pellet transplantation. Photographs of a left-TA muscle were taken. A = Step 1; B = Step 2; and C = Step 4. Dotted circle in B shows peeling of fibers. White arrows in C show partially sutured skin. Bars = 1 mm.

Figure 2. RT-PCR analysis of Sk-MSC sheet-pellet and its expressions of cytokines immediately prior to transplantation. (A) Expressions of myogenic, neurotrophic, and vasculogenic factor mRNAs was observed, confirming the quality of the sheet-pellet preparation. bp = base pair. (B) Several cytokines related to the muscle and vascular regeneration was also detected in the culture supernatant of the sheet-pellet, confirming the putative capacity of paracrine.

Figure 3. Differences of operated TA muscle mass and tetanic tension output between the short (4-8 weeks) and long (14-18 weeks) term groups, and these composed individual plots at each

measurement point. Average of operated muscle mass (A) and tetanic tension output (B) were higher in the long term group (but not significant). (C and D) Linear relationships between term and recovery are detected on the individual plots of the long term group, but not in the short term group both in the muscle mass (C) and tetanic tension output (D).

Figure 4. Macroscopic observation of surgically treated TA muscles at 5-10 weeks after transplantation *in situ* and *in vitro* (after removal). Photographs were taken by synchronizing light conditions as the fluorescence + normal. (A-G) Typical features of sheet-pellet (GFP^+) transplanted muscles. A-C = Pattern 1, D = Pattern 2, E = Pattern 3, F = Pattern 4, and G-H = Pattern 5. Arrows in B, D, E, F, G, and H show blood vessels. (I and J) Typical features of media transplanted control muscles. White arrows in panel I show the dent in the TA position. Red arrows in panel J show fat tissue. Black arrows in I and J indicate tibial bone. Bars = 1 mm.

Figure 5. Immunohistochemical detection of engrafted Sk-MSCs in cross-section (operated muscle from Pattern 1, 7 weeks after operation). (A and B) Relationship among the GFP^+ cell-derived connective tissue, recipient tendon, and muscle fibers. Skeletal muscle fibers were stained with Sk-actin (skeletal muscle actin, A), and tendon and connective tissues were stained with Elastica Van Gieson (B). (C) Endothelial cell staining with CD31. (D) Axon staining with Neurofilament 200 (N200). (E) Schwann cell staining with p75. (F) Dystrophin staining for skeletal muscle fibers in the MTJ. Muscle fibers expressing dystrophin (red reactions). T = tendon. Dotted lines in D and E show the border between connective tissue and muscle fibers. Blue staining = DAPI. Bars in A and B = 200 μm, C-E = 100 μm.

620 **Figure 6.** Immunohistochemical detection of engrafted Sk-MSCs in longitudinal sections
621 (operated muscle from Pattern 5, 8 weeks after operation). (A) Close relationship between donor-
622 derived GFP^+ connective tissue and muscle fibers was also apparent in the longitudinal images.
623 (B) GFP^+ muscle fibers were observed. (C) Vascular smooth muscle staining. (D) Axon staining
624 by N200. (E) Schwann cell staining by p75. (F) Axon and neuromuscular junction staining by
625 N200 and α-Bungarotoxin. Dotted circle in panel F shows the position of neuromuscular
626 junction. Mf = muscle fiber. Blue staining = DAPI. Bars = 100 μm.

Table 1. Specific primers for mice.

No	Gene name (full name and/or typical role)	product size (bp)	Forward primer	Reverse primer	Utilization purpose
1	**MyoD** (myogenic regulatory factors)	184	GGCCACTCAGGTCTCAGGTGT	TGTTGCACTACACAGCATGCCT	Myogenic determination and differentiation markers
2	**Myf5** (myogenic regulatory factors)	179	TTAGCAAACCATGAACACGAAACA	AAGGGGGCTTCATTTACCAGG	
3	**Pax7** (paired box transcription factors, also known as satellite cell marker)	192	CCCAACAGGTTTTCCCAACTG	CGGCCTTCTTCTAGGTTCTGCT	
4	**Pax3** (paired box transcription factors relate to embryonic muscle development)	256	TGGACAGTCTGCCCACATCTCAGC	GGGAGCCTGTGCTGTAGCAATCAG	
5	**Myogenin** (myogenic regulatory factors)	262	TACGTCCATCGTGGACAGCAT	TCAGCTAAATTCCCTCGCTGG	
6	**c-met** (hepatocyte growth factor receptor, which is present in quiescent satellite cell)	337	CCAAGCCGCGTATGTCAGTAAA	AATAAGTCGACGCGCTGCA	
7	**M-cad** (M-cadherin, a Ca2+-dependent cell adhesion molecule which is present in quiescent satellite cell)	193	GGGCTCTCTCTTGGGATGTG	CTTCTGCACTCTGCCAGGAC	
8	**MyH** (skeletal muscle myosin heavy chain, cell differentiation marker)	152	TCAGGAAAGCCCAGCATGAG	TGCACCAGGAGGTCTTGCTC	
9	**Desmin** (Muscle relate intermediate filament protein, cell differentiation marker)	106	AGGGTCAGGACCGAGTTTGTG	GCCATGAGGGCAGTTTTCAG	
10	**IGF1** (Insulin-like growth factor-1)	185	CTGCTTGCTCACCTTCACCAG	TCCGGAAGCAACACTCATCC	
11	**NGF** (Nerve growth factor, peripheral nerve growth and trophic factor)	106	TGCACCACGACTCACACCTTC	TCCTGCTGAGCACACACACAC	Peripheral nerve growth and trophic factors

12	**BDNF** (Brain-derived neurotrophic factor)	582	GGGACTCTGGAGAGCGTGAAT	CCTTATGAATCGCCAGCCAAT	
13	**GDNF** (Glial cell-derived neurotrophic factor, peripheral nerve growth and trophic factor)	180	GTGAATCGGCCGAGACAATG	CACACCGTTTAGCGGAATGC	
14	**CNTF** (Ciliary neurotrophic factor, peripheral nerve growth and trophic factor)	241	TTTCTGCCTTCGCCTACCAG	TTGGCCCCATAATGGCTCTC	
15	**LIF** (Leukemia inhibitory factor, peripheral nerve growth and trophic factor)	169	ATCGGATGGTCGCATACCTG	CCCACACGGTACTTGTTGCAC	
16	**Ninjurin** (nerve injury-induced protein)	243	GGAGCAGGGCAATGATTTCG	GCCACGTCCATTACAGGCTTC	
17	**Galectin-1** (Initial axonal growth regulator in peripheral nerves after axotomy)	109	TGTCTCAAAGTTCGGGGAGAGG	GGGCATTGAAGCGAGGATTG	
18	**Nestin** (Nerve relate intermediate filament protein, cell differentiation marker)	233	GCTCTGGGCCAGCACTCTTAG	TGTAGACAGGCAGGGCTAGCA	
19	**Sox10** (transcription factor relate to Schwann cell-development)	213	TCCCCATGTTCTTCCCATCC	CAAAGGGTGCAAGGCAAAGG	
20	**VEGF** (Vascular endothelial growth factor, vascular relating growth factor)	260	TCAGGGTTTCGGGAACCAGAC	TTCCGGGCTTGGCGATTTAG	Vascular relating growth factor
21	**HGF** (Hepatocyte growth factor, common elements to muscle and vascular growth)	169	TCAGCACCATCAAGGCAAGG	GATGGCACATCCACGACCAG	
22	**PDGF-b** (Platelet-derived growth factor-b, vascular relating growth factor)	271	AGCCAAGACGCCTCAAGCTC	GGGTGAGGGAAGCACCATTG	
23	**TGFb** (Transforming growth factor-b, vascular relating growth factor)	195	CCAAGGGCTACCATGCCAAC	ACTGCTCCACCTTGGGCTTG	
24	**EGF** (Epidermal Growth Factor, common elements to muscle and nerve growth)	137	TGCGGATGGTACGAATGGTG	GTGGAATCCAGCAGCTTTGC	
25	**FGF2** (basic fibroblast growth factor, common elements to muscle and nerve growth)	161	GCCAACCGGTACCTTGCTATG	TGCCCAGTTCGTTTCAGTGC	
26	**HPRT** (hypoxanthine guanine phosphoribosyl transferase)	111	GCAAACTTTGCTTTCCCTGGTTAAG	CAACAAAGTCTGGCCTGTATCCA	House-keeping control gene

627 Table 2. Functional assessment of the operated muscle

Experimental group		Short term (4-8 weeks) recovery group (n=4)		Long term (14-18 weeks) recovery group (n=4)	
		Muscle mass (mg)	Tetanic tension N ($1x10^2$)	Muscle mass (mg)	Tetanic tension N ($1x10^2$)
SP group (n=8)	Op-side	29.0±6.3	25.5±7.4	38.9±4.9	37.4±9.7
	Cont-side	45.2±5.8	71.1±15.8	50.4±0.5	75.8±11.8
	Recovery ratio	64%	36%	77%	49%
C group (n=5)	Op-side	unmeasurable	unmeasurable	nd	nd
	Cont-side	51.6±0.7	79.7±3.8	nd	nd
	Recovery ratio	0	0	nd	nd

628 Values are expressed average ±SE. *$p<0.05$ 4-weeks vs. 10 weeks tetanus.

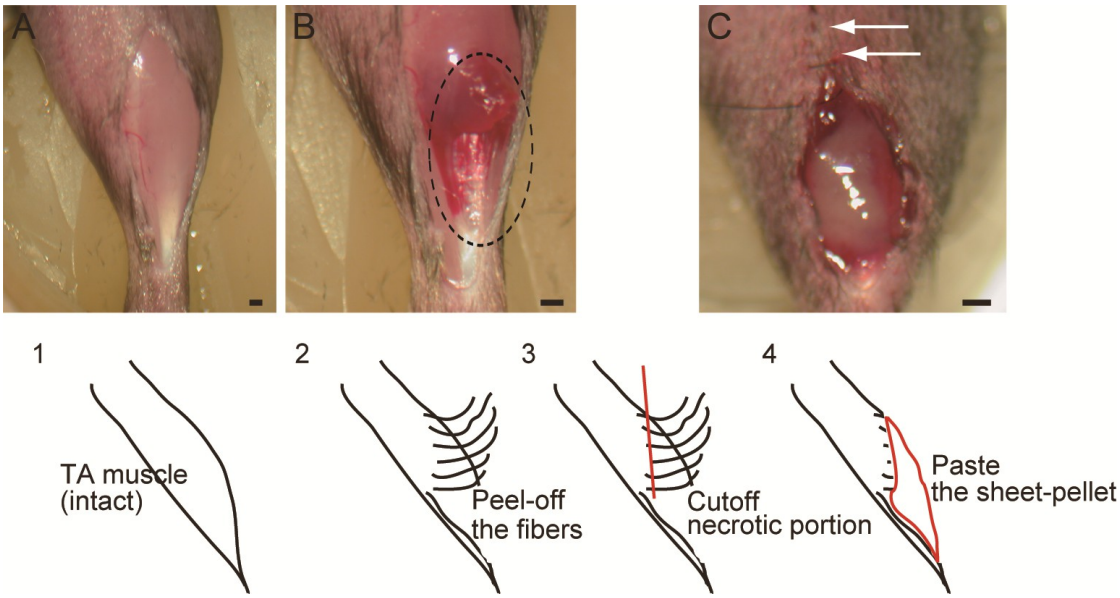

Figure 1. Macroscopic and schematic images of procedures used in MTJ complete rupture model preparation and sheet-pellet transplantation. Photographs of a left-TA muscle were taken. A = Step 1; B = Step 2; and C = Step 4. Dotted circle in B shows peeling of fibers. White arrows in C show partially sutured skin. Bars = 1 mm.

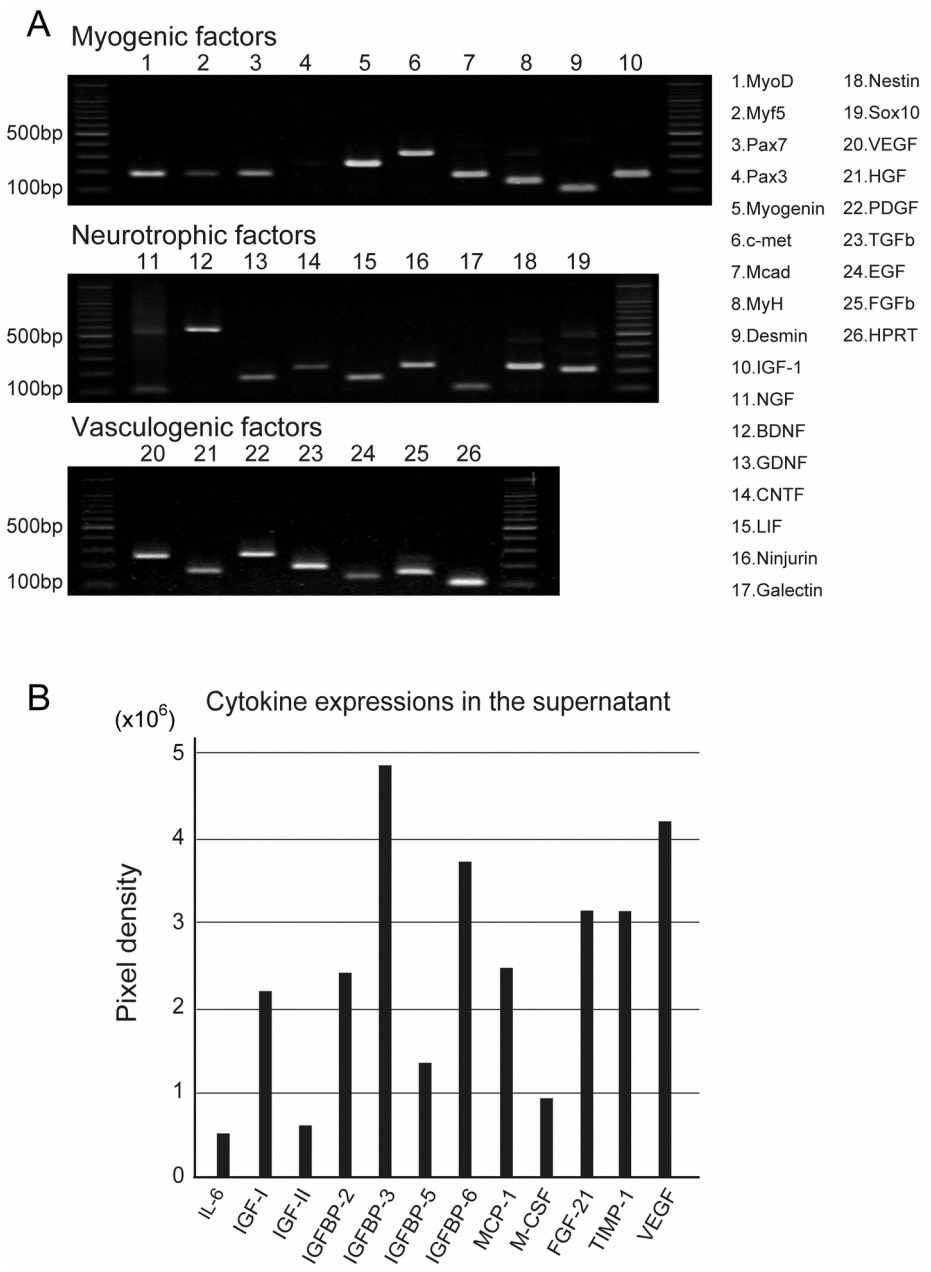

633 **Figure 2.** RT-PCR analysis of Sk-MSC sheet-pellet and its expressions of cytokines immediately
634 prior to transplantation. (A) Expressions of myogenic, neurotrophic, and vasculogenic factor
635 mRNAs was observed, confirming the quality of the sheet-pellet preparation. bp = base pair. (B)
636 Several cytokines related to the muscle and vascular regeneration was also detected in the culture
637 supernatant of the sheet-pellet, confirming the putative capacity of paracrine.

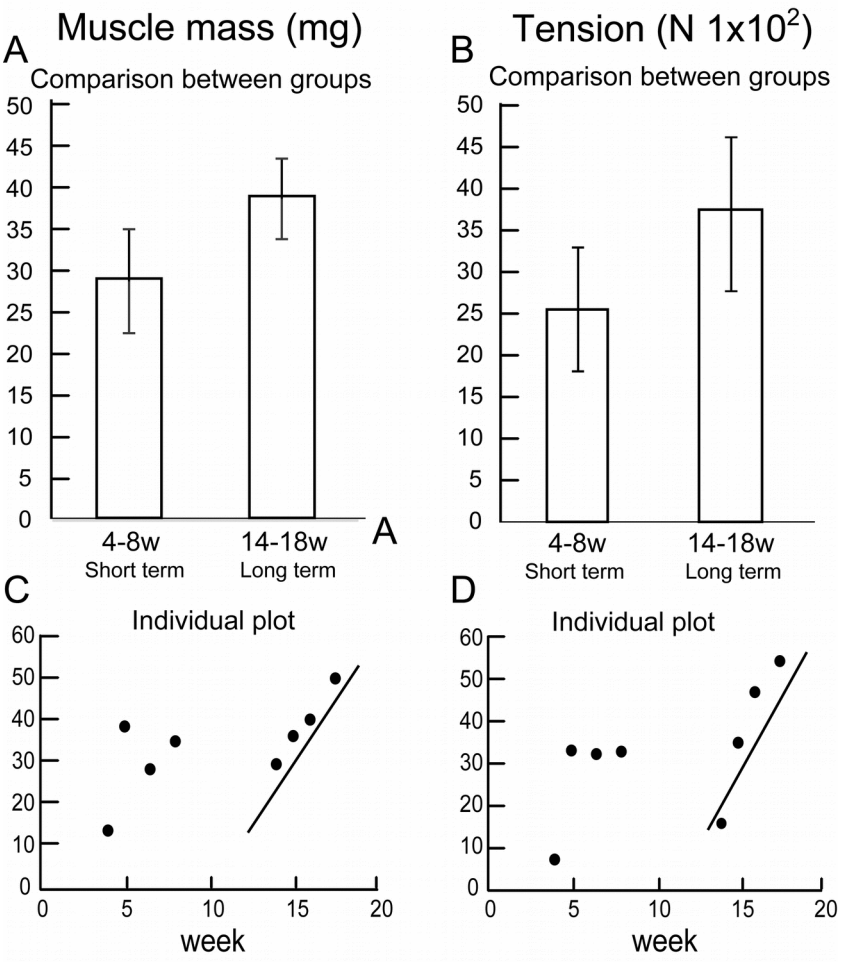

638 **Figure 3.** Differences of operated TA muscle mass and tetanic tension output between the short
639 (4-8 weeks) and long (14-18 weeks) term groups, and these composed individual plots at each
640 measurement point. Average of operated muscle mass (A) and tetanic tension output (B) were
641 higher in the long term group (but not significant). (C and D) Linear relationships between term
642 and recovery are detected on the individual plots of the long term group, but not in the short term
643 group both in the muscle mass (C) and tetanic tension output (D).

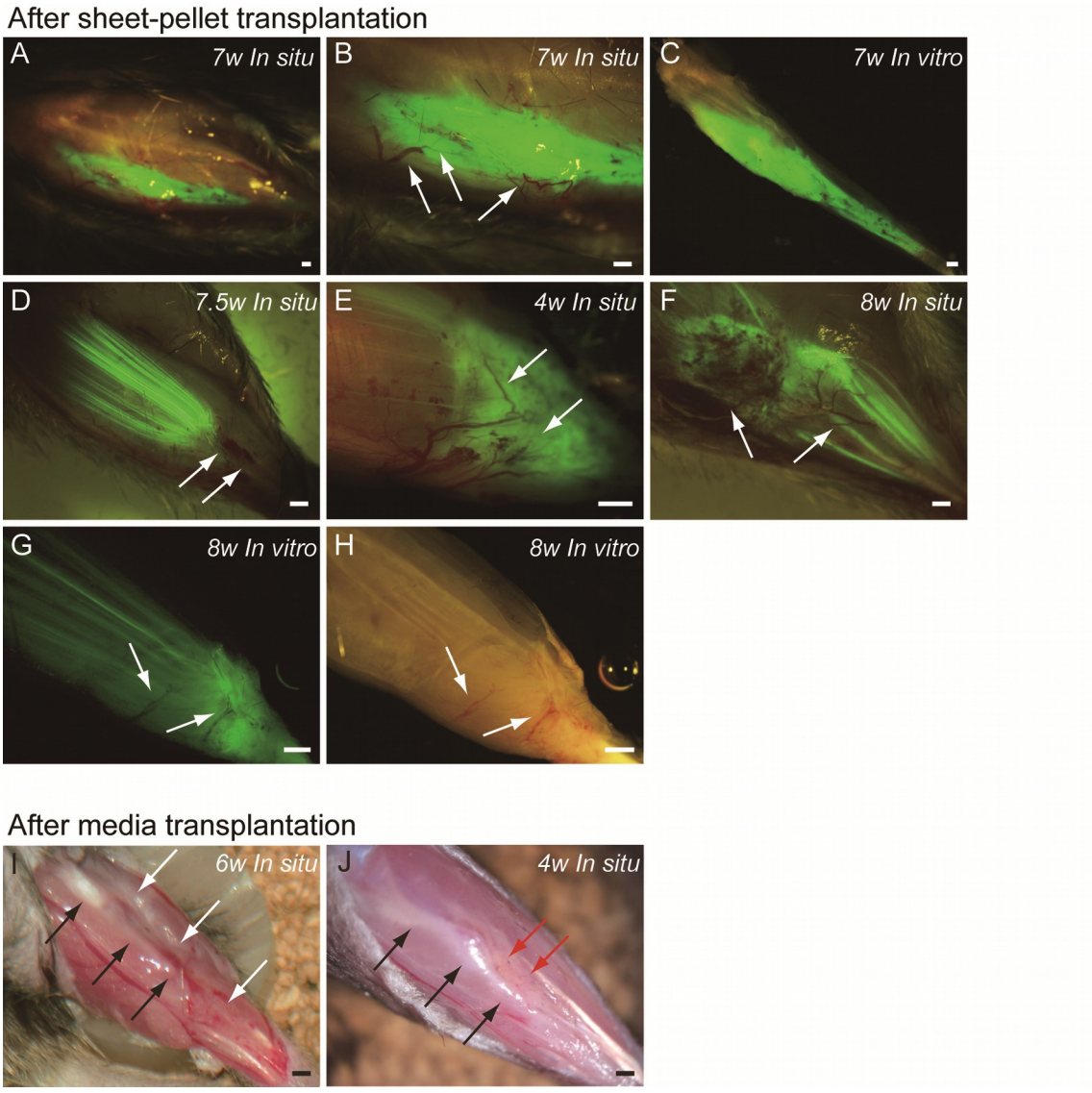

644 **Figure 4.** Macroscopic observation of surgically treated TA muscles at 5-10 weeks after
645 transplantation *in situ* and *in vitro* (after removal). Photographs were taken by synchronizing light
646 conditions as the fluorescence + normal. (A-G) Typical features of sheet-pellet (GFP^+)
647 transplanted muscles. A-C = Pattern 1, D = Pattern 2, E = Pattern 3, F = Pattern 4, and G-H =
648 Pattern 5. Arrows in B, D, E, F, G, and H show blood vessels. (I and J) Typical features of media
649 transplanted control muscles. White arrows in panel I show the dent in the TA position. Red
650 arrows in panel J show fat tissue. Black arrows in I and J indicate tibial bone. Bars = 1 mm.

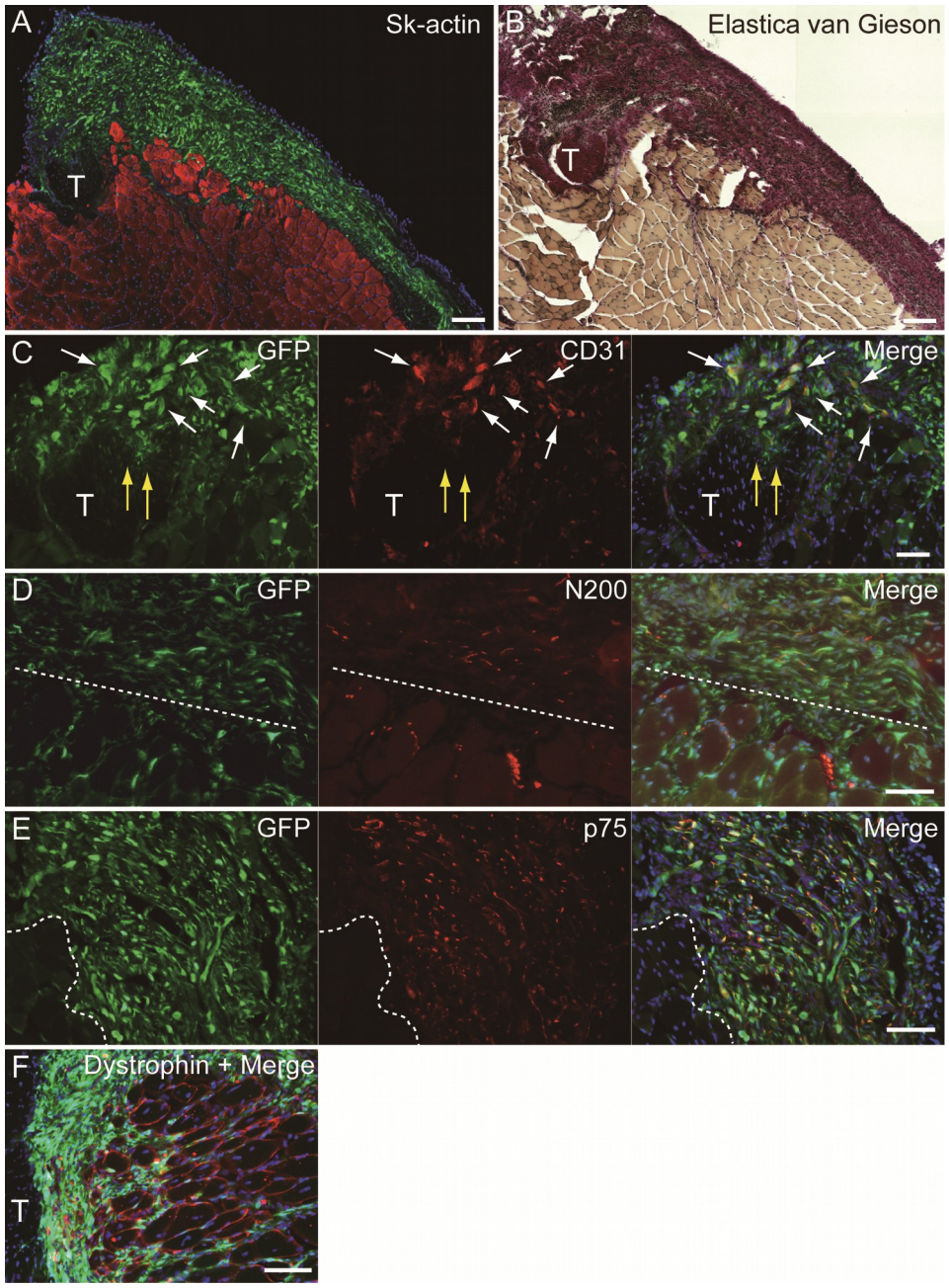

Figure 5. Immunohistochemical detection of engrafted Sk-MSCs in cross-section (operated muscle from Pattern 1, 7 weeks after operation). (A and B) Relationship among the GFP^+ cell-derived connective tissue, recipient tendon, and muscle fibers. Skeletal muscle fibers were stained with Sk-actin (skeletal muscle actin, A), and tendon and connective tissues were stained with Elastica Van Gieson (B). (C) Endothelial cell staining with CD31. (D) Axon staining with Neurofilament 200 (N200). (E) Schwann cell staining with p75. (F) Dystrophin staining for skeletal muscle fibers in the MTJ. Muscle fibers expressing dystrophin (red reactions). T = tendon. Dotted lines in D and E show the border between connective tissue and muscle fibers. Blue staining = DAPI. Bars in A and B = 200 μm, C-E = 100 μm.

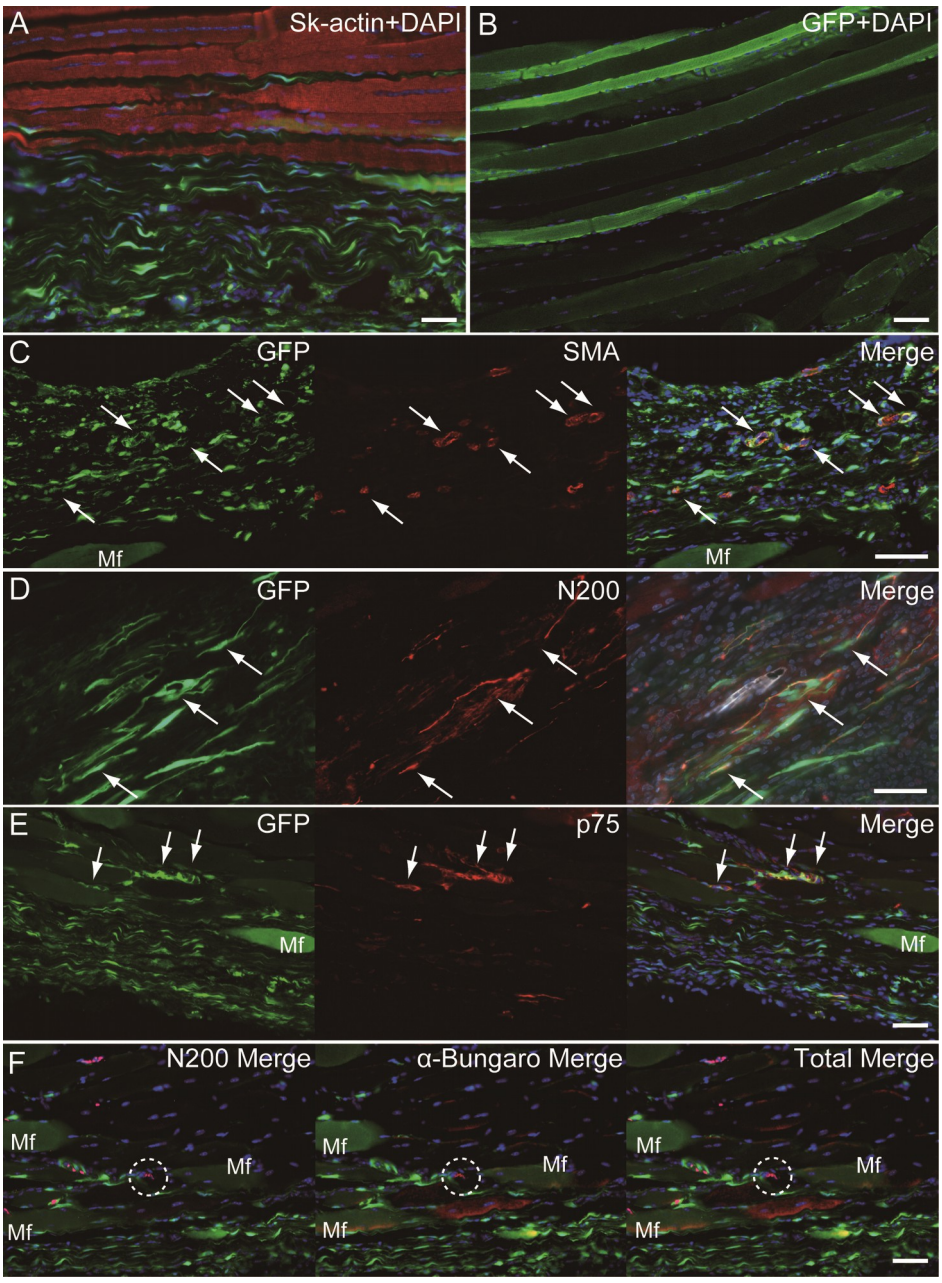

660 **Figure 6.** Immunohistochemical detection of engrafted Sk-MSCs in longitudinal sections
661 (operated muscle from Pattern 5, 8 weeks after operation). (A) Close relationship between donor-
662 derived GFP^+ connective tissue and muscle fibers was also apparent in the longitudinal images.
663 (B) GFP^+ muscle fibers were observed. (C) Vascular smooth muscle staining. (D) Axon staining
664 by N200. (E) Schwann cell staining by p75. (F) Axon and neuromuscular junction staining by
665 N200 and α-Bungarotoxin. Dotted circle in panel F shows the position of neuromuscular
666 junction. Mf = muscle fiber. Blue staining = DAPI. Bars = 100 μm.